Physics of Plasmas ARTICLE pubs.aip.org/aip/pop

Bound state energies and critical bound region in the semiclassical dense hydrogen plasmas

Cite as: Phys. Plasmas **31**, 042110 (2024); doi: 10.1063/5.0185339
Submitted: 30 October 2023 · Accepted: 22 March 2024 ·
Published Online: 9 April 2024

Tong Yan,[1,2] Li Guang Jiao,[2,3,4,a)] Aihua Liu,[1,a)] Yuan Cheng Wang,[3,4,5] Henry E. Montgomery, Jr.,[6] Yew Kam Ho,[7] and Stephan Fritzsche[3,4,8]

AFFILIATIONS

[1]Institute of Atomic and Molecular Physics, Jilin University, Changchun 130012, People's Republic of China
[2]College of Physics, Jilin University, Changchun 130012, People's Republic of China
[3]Helmholtz-Institut Jena, D-07743 Jena, Germany
[4]GSI Helmholtzzentrum für Schwerionenforschung GmbH, D-64291 Darmstadt, Germany
[5]College of Physical Science and Technology, Shenyang Normal University, Shenyang 110034, People's Republic of China
[6]Chemistry Program, Centre College, Danville, Kentucky 40422, USA
[7]Institute of Atomic and Molecular Sciences, Academia Sinica, Taipei 10617, Taiwan, Republic of China
[8]Theoretisch-Physikalisches Institut, Friedrich-Schiller-Universität Jena, D-07743 Jena, Germany

[a)]**Authors to whom correspondence should be addressed:** lgjiao@jlu.edu.cn and aihualiu@jlu.edu.cn

ABSTRACT

We calculate the bound state energies of the hydrogen atom in semiclassical dense hydrogen plasmas modeled by the effective screened interaction potential developed by Ramazanov *et al.* [Phys. Rev. E **92**, 023104 (2015)]. It is shown that the quantum degenerate and exchange-correlation effects of plasma electrons do not play significant roles in the region where the system exhibits bound states. The bound-continuum critical transition lines and the distribution of the ground state energies in the plasma density-temperature phase diagrams are obtained, both with and without taking into account the screening effect of the plasma ions. The dipole transition oscillator strengths and static dipole polarizabilities of the electron-ion subsystems in semiclassical dense hydrogen plasmas are calculated in a wide range of plasma parameters.

I. INTRODUCTION

Investigation of the spectral properties and collisional dynamics of the electron-ion subsystems in plasmas has attracted considerable interest in recent years due to their great importance in modeling the microscopic and thermodynamic processes in plasmas and diagnosing plasma parameters such as temperature and density.[1–3] During recent years, significant progress has been made by many authors to determine, e.g., accurate bound state energies, transition amplitudes, multipole polarization properties, electron impact excitation and ionization scattering cross sections, and laser-induced nonlinear responses of the electron-ion subsystems embedded in different plasma environments.[4–16] The most widely investigated plasmas are probably the weakly coupled ideal plasmas, in which the effective interaction potential between a pair of charged particles is modeled by the Debye–Hückel potential.[17] In that model, the Coulomb interaction is screened by an exponential factor with a length parameter called the Debye length,[2] beyond which plasma particles effectively screen any localized charge imbalance. The strongly coupled plasmas, in the opposite limit, generally have low temperatures and high electron densities, and the screening effect is better described by the ion-sphere model.[18] In such an approximation, each stationary ion is surrounded by electrons uniformly distributed in a Wigner–Seitz sphere to neutralize the ionic charge.

In dense plasmas, the quantum degenerate effect of electrons is measured by the ratio of thermal energy to the Fermi energy of electrons.[19] For dense plasmas in the fully degenerate region, where energies of degenerate electrons follow the Fermi–Dirac distribution, a novel attractive interaction potential between charged particles was

derived by Shukla and Eliasson[20–22] and later improved by Akbari-Moghanjoughi *et al.*[23–25] considering both the quantum statistical pressure and the quantum Bohm potential, as well as the electron exchange-correlation effects. A simplified model, which is called the modified Debye–Hückel or exponential cosine screened Coulomb potential[26] attracted special interest in subsequent investigations, partially due to its simple analytical formalism. On the other hand, the semiclassical dense plasmas have attracted growing interest in recent years due to their importance for understanding the evolution of stellar interiors and the extreme environment in inertial confinement fusion.[2,27,28] The recent works of Ramazanov *et al.*[29–32] made a major step forward in developing compact and analytical effective interaction potentials between charged particles in these weakly nonideal, semiclassical dense plasmas. Based on the Deutsch micropotential[33] and the static dielectric function in the linear response approximation, Ramazanov *et al.*[32] developed a new screened interaction potential between charged particles by taking into account both the quantum mechanical diffraction and symmetry effects between colliding particles at short distances, and the simultaneous screening effects of plasma electrons and ions.[32] Such a model potential successfully treats the effective interactions of the electron–electron, ion–ion, and electron-ion subsystems in a unified framework.

Since the development of the Ramazanov effective interaction potential, this model potential and corresponding variants have been widely employed to investigate various thermodynamic and transport properties of nonideal semiclassical dense plasmas, including the scattering of electrons from ions and atoms,[34–39] the optical reflectivity,[40] relaxation of plasma temperature and coupling parameters,[41,42] dynamical conductivity,[43,44] Coulomb logarithm and stopping power,[45–47] etc. In a recent work, Shalenov *et al.*[48] calculated the bound state energy spectra of the hydrogen atom under the Ramazanov model potential using the Ritz variational method. It has been shown that the electron degeneracy and plasma screening effects lead to a decrease in the ionization potentials, and in the high-density limit, system bound energies approach zero and eventually bound states merge into the continuum.[48] Such a phenomenon is called the pressure ionization in plasmas[49,50] or Mott transition in condensed matter.[51] The bound-continuum transition has a close relationship to the quantum phase transition and symmetry breaking of electron configuration and also appears in other physical systems with potentials having adjustable parameters.[52–56] Investigation of the shifts of bound state energies and accurate positions of the continuum edge attracts wide interest in a variety of plasmas, and so far they have not been established in the semiclassical dense region. The purpose of this work is first to provide alternative and accurate solutions of the bound state energies of the hydrogen atom in semiclassical dense hydrogen plasmas and second to determine the critical bound region where bound-continuum phase transition occurs.

The rest of this paper is structured as follows: In Sec. II, we introduce the Ramazanov model potential for simulating the electron-ion interaction in semiclassical dense plasmas, the definition of plasma parameters, the valid range of the potential, and the numerical method for calculating the bound state energies. In Sec. III, we compare the present results with previous calculations and make a comprehensive survey of the critical bound region for the electron-ion subsystem in plasmas. Physical properties of dipole transition oscillator strengths and static polarizabilities for the ground state of the system are also investigated in Sec. III. Section IV gives a summary of the present work. Both atomic units ($\hbar = m_e = e = 1$) and those more widely used in plasma physics (e.g., eV and cm^{-3} for the plasma temperature and particle number density, respectively) will be used according to circumstances.

II. THEORETICAL METHOD

A. Effective interaction potential

The electron-ion effective interaction potential in the semiclassical dense plasmas was derived by Ramazanov *et al.*[32] using the Deutsch micropotential[33] and the dielectric response function in a linear response approximation. The potential is expressed in a compact form

$$V_{ei}(r) = -\frac{Ze^2}{r\sqrt{(1+k_i^2\lambda_{ee}^2)^2 - 4k_D^2\lambda_{ee}^2}}\left(\left(\frac{1-\lambda_{ee}^2B^2}{1-\lambda_{ei}^2B^2}\right)e^{-Br} - \left(\frac{1-\lambda_{ee}^2A^2}{1-\lambda_{ei}^2A^2}\right)e^{-Ar}\right) + \frac{Ze^2}{r(1+C_{ei})}e^{-\frac{r}{\lambda_{ei}}}, \tag{1}$$

where

$$A^2 = \frac{1+k_i^2\lambda_{ee}^2 + \sqrt{(1+k_i^2\lambda_{ee}^2)^2 - 4k_D^2\lambda_{ee}^2}}{2\lambda_{ee}^2}, \tag{2}$$

$$B^2 = \frac{1+k_i^2\lambda_{ee}^2 - \sqrt{(1+k_i^2\lambda_{ee}^2)^2 - 4k_D^2\lambda_{ee}^2}}{2\lambda_{ee}^2}, \tag{3}$$

$$C_{ei}^2 = \frac{k_D^2\lambda_{ei}^2 - k_i^2\lambda_{ee}^2}{\lambda_{ee}^2/\lambda_{ei}^2 - 1}, \tag{4}$$

and

$$k_D^2 = k_i^2 + k_e^2. \tag{5}$$

In the formulas above, $k_i = \sqrt{4\pi n_i Z_i^2 e^2/(k_B T_i)}$ and $k_e = \sqrt{4\pi n_e e^2/(k_B T_e)}$ represent the wave numbers of the plasma ions and electrons, respectively. Z_i is the electronic charge of the ions, and $T_{i(e)}$ $n_{i(e)}$ are, respectively, the temperature and density of the plasma ions (electrons). $\lambda_{ei} = \hbar/\sqrt{2\pi\mu_{ei}k_B T_{ei}}$ is the thermal de Broglie wavelength of pairs of electron and ion, in which $\mu_{ei} = m_e m_i/(m_e + m_i)$ is the electron-ion reduced mass and $T_{ei} = \sqrt{T_e T_i}$ is the temperature of the electron-ion subsystem. The thermal de Broglie wavelengths $\lambda_{ee} = \hbar/\sqrt{2\pi m_e k_B T_e}$ and $\lambda_{ii} = \hbar/\sqrt{2\pi m_i k_B T_i}$ are employed for electrons and ions, respectively, while in deriving Eq. (1), it has been assumed that ions are point-like particles, i.e., $\lambda_{ii} = 0$, due to $m_i \gg m_e$. We note that there exists a debate on the different choice of the wavelength λ_{ei} in the literature (see, e.g., Refs. 42, 57, and 58 for discussion), and the original formulations of the Deutsch potential were also published in different forms by the authors.[33,59–62] As we will explain later, λ_{ei} will be omitted in our following calculations of the bound state energies of the electron-ion subsystem. In this work, we focus on hydrogen plasmas in the thermodynamic equilibrium condition, i.e., $Z_i = 1$, $T_e = T_i$, and therefore, $n_e = Z_i n_i = n_i$.

It should be mentioned that in the recent works of Kodanova *et al.*[42] and Shalenov *et al.*,[48] those authors employed a different definition of the electron wavelength λ_{ee} by incorporating the electron degeneracy and exchange-correlation effect [see Eq. (2) in Ref. 48 for

more details]. Here, we simplify our calculations by directly using the original thermal de Broglie wavelength of electrons. In the results and discussion, we will show that such a simplification does not produce a significant effect on the physical properties investigated in this work.

Despite the different choices of the wavelength parameters, the electron-ion pair interaction potential given in Eq. (1) takes into account the quantum effects of diffraction and symmetry between the colliding charged particles at short distances, and therefore, it can be properly used to model the collisional dynamics in the semiclassical dense plasmas. It was, however, pointed out by Shalenov *et al.*[48] that when using Eq. (1) in solving the Schrödinger equation of the electron-ion subsystem, double counting of the quantum diffraction effect arises due to the explicit appearance of the parameter λ_{ei} in the Deutsch micropotential. Therefore, to calculate the bound state energies of the electron-ion subsystem, one should rewrite Eq. (1) by setting $\lambda_{ei} = 0$, which yields

$$V_{ei}(r) = -\frac{Ze^2}{r\sqrt{(1+k_i^2\lambda_{ee}^2)^2 - 4k_D^2\lambda_{ee}^2}} \times \left(\left(1-\lambda_{ee}^2B^2\right)e^{-Br} - \left(1-\lambda_{ee}^2A^2\right)e^{-Ar}\right). \quad (6)$$

This potential, if a further approximation is made without taking into account the screening effect of the ionic components ($k_i = 0$), recasts the potential derived by Stanton and Murillo[63] based on the finite-temperature orbital-free density functional theory. Throughout this work, we will employ Eq. (6) as the model potential to investigate the bound state energies of the electron-ion subsystem, both with ($k_i \neq 0$) and without ($k_i = 0$) considering the screening effect of ions. Some examples of the potential parameters λ_{ee}, k_e, A, and B for $k_i \neq 0$ at some selected values of plasma temperatures and densities are given in Table I for reference.

B. Plasma parameters

To simplify our calculation and the following discussion, plasmas are characterized by three dimensionless parameters. The electron density parameter is given by

$$r_s = \frac{a_e}{a_B}, \quad (7)$$

where $a_e = (3/(4\pi n_e))^{1/3}$ is the average distance between electrons and a_B is the in bohr radius. The electron degeneracy parameter is defined as

TABLE I. Parameters of the electron-ion effective interaction potential in Eq. (6) with considering the screening effect of ions ($k_i \neq 0$) at some selected values of plasma temperatures and densities. For the hydrogen plasmas in thermodynamic equilibrium where $Z_i = 1$, $T_i = T_e$, and $n_i = n_e$, it simplifies that $k_e = k_i$ and $k_D = \sqrt{2}k_e$. Those places without data represent the potential in the forbidden region [see Eq. (15)]. Numbers in parentheses represent powers of ten.

$n_e(\mathrm{cm}^{-3})$	r_s	θ	Γ	$k_e = k_i$	A	B
			$k_BT_e = 50$ ($\lambda_{ee} = 0.294\,306\,868\,062$)			
1×10^{21}	1.172 292 53(1)	1.371 196 62(2)	4.642 422 53(−2)	3.183 442 15(−2)	3.397 664 85	4.502 264 71(−2)
1×10^{23}	2.525 627 69	6.364 530 92	2.154 821 66(−1)	3.183 442 15(−1)	3.382 598 03	4.522 318 77(−1)
1×10^{25}	5.441 299 91(−1)	2.954 153 56(−1)	1.000 179 61	3.183 442 15	–	–
			$k_BT_e = 100$ ($\lambda_{ee} = 0.208\,106\,382\,157$)			
1×10^{21}	1.172 292 53(1)	2.742 393 24(2)	2.321 211 27(−2)	2.251 033 53(−2)	4.805 181 93	3.183 477 09(−2)
1×10^{23}	2.525 627 69	1.272 906 18(1)	1.077 410 83(−1)	2.251 033 53(−1)	4.799 935 91	3.186 956 42(−1)
1×10^{25}	5.441 299 91(−1)	5.908 307 13(−1)	5.000 898 07(−1)	2.251 033 53	–	–
			$k_BT_e = 200$ ($\lambda_{ee} = 0.147\,153\,434\,031$)			
1×10^{21}	1.172 292 53(1)	5.484 786 48(2)	1.160 605 63(−2)	1.591 721 08(−2)	6.795 609 38	2.251 039 71(−2)
1×10^{23}	2.525 627 69	2.545 812 37(1)	5.387 054 14(−2)	1.591 721 08(−1)	6.793 761 60	2.251 651 95(−1)
1×10^{25}	5.441 299 91(−1)	1.181 661 43	2.500 449 04(−1)	1.591 721 08	6.581 132 01	2.324 400 51
			$k_BT_e = 400$ ($\lambda_{ee} = 0.104\,053\,191\,078$)			
1×10^{21}	1.172 292 53(1)	1.096 957 30(3)	5.803 028 16(−3)	1.125 516 77(−2)	9.610 462 72	1.591 722 17(−2)
1×10^{23}	2.525 627 69	5.091 624 73(1)	2.693 527 07(−2)	1.125 516 77(−1)	9.609 810 04	1.591 830 28(−1)
1×10^{25}	5.441 299 91(−1)	2.363 322 85	1.250 224 52(−1)	1.125 516 77	9.542 435 59	1.603 069 41
			$k_BT_e = 800$ ($\lambda_{ee} = 0.073\,576\,717\,016$)			
1×10^{21}	1.172 292 53(1)	2.193 914 59(3)	2.901 514 08(−3)	7.958 605 38(−3)	1.359 125 37(1)	1.125 516 96(−2)
1×10^{23}	2.525 627 69	1.018 324 95(2)	1.346 763 54(−2)	7.958 605 38(−2)	1.359 102 30(1)	1.125 536 07(−1)
1×10^{25}	5.441 299 91(−1)	4.726 645 70	6.251 122 59(−2)	7.958 605 38(−1)	1.356 777 28(1)	1.127 464 83
			$k_BT_e = 1000$ ($\lambda_{ee} = 0.065\,809\,016\,323$)			
1×10^{21}	1.172 292 53(1)	2.742 393 24(3)	2.321 211 27(−3)	7.118 393 06(−3)	1.519 548 45(1)	1.006 692 91(−2)
1×10^{23}	2.525 627 69	1.272 906 18(2)	1.077 410 83(−2)	7.118 393 06(−2)	1.519 531 95(1)	1.006 703 85(−1)
1×10^{25}	5.441 299 91(−1)	5.908 307 13	5.000 898 07(−2)	7.118 393 06(−1)	1.517 873 01(1)	1.007 804 11

$$\theta = \frac{k_B T_e}{E_F}, \tag{8}$$

where $E_F = \hbar^2 (3\pi^2 n_e)^{2/3}/(2m_e)$ is the Fermi energy of electrons. For $\theta \ll 1$, the plasma is classified as a degenerate quantum plasma, while for $\theta \gg 1$, the plasma is considered as a non-degenerate classical plasma. The semiclassical plasmas are generally defined in the transition region between them. The Coulomb coupling parameter reads

$$\Gamma = \frac{e^2}{a_e k_B T_e}. \tag{9}$$

When $\Gamma \ll 1$, the electrons are said to be weakly coupled, while $\Gamma \gg 1$ means the electrons are strongly coupled. These three dimensionless parameters are not independent, since the electron degeneracy parameter θ and Coulomb coupling parameter Γ can be connected via the electron density parameter r_s through

$$\theta\Gamma = \frac{e^2}{a_e E_F} \approx 0.543011\, r_s. \tag{10}$$

The characteristic plasma parameters, which are more extensively used in plasma experiments, i.e., the plasma particle density and temperature, can be derived straightforwardly as

$$n_e = \frac{3}{4\pi} r_s^{-3} \approx 0.238732\, r_s^{-3}\ (\text{a.u.}) \approx 1.611046 \times 10^{24}\, r_s^{-3}\ (\text{cm}^{-3}), \tag{11}$$

and

$$k_B T_e = \frac{1}{2}\left(\frac{9\pi}{4}\right)^{\frac{2}{3}} \theta r_s^{-2} \approx 1.841584\, \theta r_s^{-2}\ (\text{a.u.}) \approx 50.11206\, \theta r_s^{-2}\ (\text{eV}). \tag{12}$$

C. Potential valid range

It can be inferred from both Eqs. (1) and (6) that such an electron-ion interaction potential can only be valid under the condition

$$1 + k_i^2 \lambda_{ee}^2 > 2 k_D \lambda_{ee}. \tag{13}$$

For plasmas that do not follow the above condition, Ramazanov *et al.*[32] provided a modified effective interaction potential to remove the imaginary unit. In this work, we solely focus on the electron-ion interaction under the above restriction, but keep in mind that another form of potential can be used in the complementary area.

The combination of Eqs. (7), (8), and (13) yields the valid range of the electron-ion potential for $k_i \neq 0$,

$$r_s > 41.399\, \theta^2 \text{ or } r_s < 1.2187\, \theta^2. \tag{14}$$

They can also be expressed in terms of the plasma density and temperature parameters as

$$n_e > 2.9142\, (k_B T_e)^2 \quad \text{or} \quad n_e < 0.0858\, (k_B T_e)^2. \tag{15}$$

For example, if $r_s = 2$, the plasma degeneracy parameter can only be set in the range of $\theta > 1.29$ or $\theta < 0.22$. On the other hand, if $k_i = 0$, i.e., $k_D = k_e$, the valid range of the potential simplifies to

$$r_s < 1.7757\, \theta^2, \tag{16}$$

or

$$n_e < 0.125\, (k_B T_e)^2. \tag{17}$$

D. Numerical calculation

The bound state energies of the electron-ion subsystem are calculated by solving the non-relativistic radial Schrödinger equation in the form

$$\left[-\frac{1}{2}\frac{d^2}{dr^2} + \frac{l(l+1)}{2r^2} + V_{ei}(r)\right]\psi_{nl}(r) = E_{nl}\psi_{nl}(r), \tag{18}$$

where V_{ei} is given by Eq. (6) and E_{nl} is the eigenenergy of the system with principal quantum number n and orbital angular momentum l. The critical bound region for the electron-ion subsystem indicates the plasma parameter region (either in terms of r_s and θ or n_e and $k_B T_e$) where the lowest eigenenergy of the system is negative, i.e.,

$$E_{1s}(r_s, \theta) < 0 \quad \text{or} \quad E_{1s}(n_e, k_B T_e) < 0. \tag{19}$$

The parameters that produce exactly zero ground state energy are defined as the critical plasma parameters.

In general, the effective electron-ion potential can be treated as a combination of two screened-type Coulomb potentials and, unfortunately, it has no known analytical solutions. In this work, we employ the generalized pseudospectral (GPS) method[64–66] to solve Eq. (18) in the discrete variable representation. The GPS method has been extensively employed in our previous work[11,12] to solve the bound state energies, wave functions, and corresponding transition and polarization properties of atoms under different screened Coulomb potentials. One of the great advantages of the GPS method is that it converges exponentially fast with a gradual increase in the dimension of discretization. This is much faster than the traditional finite-basis-set expansion methods and the finite-difference or finite-element methods.[67] Such computational superiority demonstrates the utility of the GPS method as a powerful tool to calculate the critical screening parameters of potentials and investigate the critical (bound-continuum and bound-resonance) transitions of quantum systems. For a detailed implementation of the GPS method in solving the radial Schrödinger equation, interested readers are referred to Refs. 64–66. The strategy of accurately determining the critical screening parameters is available in Refs. 68–70.

III. RESULTS AND DISCUSSION

A. Effective potential and ground state energies

To validate the effective potentials used in the present numerical calculations, we reproduce the potential curves described in Eqs. (1) and (6) in Figs. 1(a) and 1(b), respectively. Figure 1(a) displays the comparison of the electron-ion effective potential derived by Ramazanov *et al.*,[32] the original Deutsch micropotential (in the limit without plasma screening, i.e., $k_i \to 0$, $k_e \to 0$, and $k_D \to 0$), and the widely used Debye potential (in the limit without quantum effects, i.e., $\lambda_{ee} \to 0$ and $\lambda_{ei} \to 0$). We successfully reproduce the three potential curves obtained by Ramazanov *et al.*[32] at $r_s = 2$ and $\theta = 2.2$ (see Fig. 3 in Ref. 32), which corresponds to the electron degeneracy parameter at about $\Gamma = 0.5$. Figure 1(b) displays the effective potentials of Eq. (6)

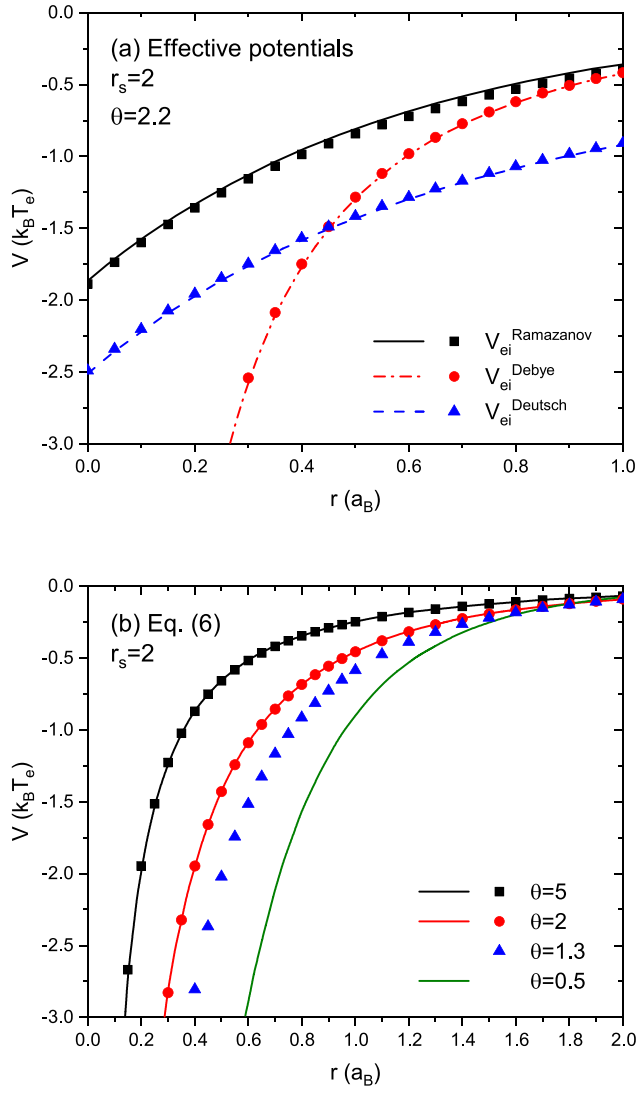

FIG. 1. Effective potential energy curves of the electron-ion system in semiclassical dense plasmas. (a) Comparison of the potential of Eq. (1) at $r_s = 2$ and $\theta = 2.2$ with the Debye and Deutsch potentials. Dots are the present calculations and lines are from Ref. 32. The expressions of the Debye and Deutsch potentials are given, respectively, in Eqs. (13) and (1) in Ref. 32. (b) Comparison of the potentials of Eq. (6) at $r_s = 2$ and some selected values of θ. Dots are the present calculations and lines are from Ref. 48. In the present models, the value of θ must be larger than 1.29 for $r_s = 2$ (see the discussion in Sec. II C).

that will be used in the following numerical solution of the Schrödinger equation. For $r_s = 2$, we successfully reproduce the potential curves obtained by Shalenov *et al.*[48] at $\theta = 5$ and 2. However, those authors used a different definition of the electron wavelength λ_{ee} by incorporating the electron quantum degeneracy and exchange-correlation effects, while we directly employ the thermal de Broglie wavelength of electrons. It can be seen that the difference is nearly indistinguishable in the current figure scale, which means that the quantum degeneracy and exchange-correlation effect do not play significant roles in the plasmas considered here. Discrepancies do exist in the valid range of the effective potential. As we have discussed in Sec. II C, if the thermal de Broglie wavelength of electrons is used in the calculation, the effective potential is restricted to the ranges of $\theta > 1.29$ and $\theta < 0.22$ for $r_s = 2$. Therefore, in Fig. 1(b) we only show the potential curves for θ as small as 1.3, while in the work of Shalenov *et al.*,[48] those authors provided the potential curve at $\theta = 0.5$. It should be kept in mind that this is in the region of weakly degenerate quantum plasmas.

The ground state energies of the electron-ion subsystem are solved by employing the GPS method. The numerical results are shown in Tables II and III for $k_i \neq 0$ and $k_i = 0$, respectively, in a wide range of dimensionless parameters r_s and θ. The implementation details of the GPS method are available elsewhere[64–66] and are omitted here. All numerical calculations can be converged to an accuracy close to the precision of numerical arithmetic with a moderate dimension of discretization.[11] For simplicity, we only show the first 6 significant digits in these tables. It is also worth mentioning that in Table II, i.e., $k_i \neq 0$, the ground state is still bound at smaller values of θ (< 1) and some large values of r_s (>5). These energies are not included in the table since the plasma electrons are in the degenerate quantum region.

Two common behaviors can be observed from the comparison shown in Tables II and III. At fixed values of r_s (i.e., fixed electron density n_e), the ground state energy increases monotonically with decreasing θ (i.e., decreasing the plasma temperature $k_B T_e$). This is consistent with the fact that in lower temperatures, the Debye length of plasmas (which characterizes the average screening distance between charged particles) is much smaller and the quantum diffraction effect becomes more important. All these effects produce a stronger screening effect on the effective interaction potential and, consequently, the bound state energies are shifted to higher levels (i.e., far away from the free hydrogen levels). At fixed values of θ, the gradual increase in r_s corresponds to the decrease in electron density n_e. As a result, the electron-ion subsystem behaves like a free hydrogen atom, and the ground state energy approaches -0.5 (in atomic units).

The validation of the present numerical results and comparison with previous calculations can be seen in Fig. 2, where for the ease of comparison the ground state energies are depicted as a function of electron density n_e, at some fixed values of temperature $k_B T_e$. Figures 2(a) and 2(b) compare the energies under potentials with $k_i \neq 0$ and $k_i = 0$, respectively. The parameters of the effective interaction potentials in Fig. 2(a) at $n_e = 1 \times 10^{21}$, 1×10^{23}, and 1×10^{25} cm^{-3} have been given in Table I. Those parameters for $k_i = 0$ in Fig. 2(b) can be obtained in a similar way by setting $k_D = k_e$. In both figures, the variational calculations of Shalenov *et al.*[48] based on the hydrogen-like wave functions are included for comparison. For $k_i = 0$, the predictions of Chen *et al.*[13] using the Stanton–Murillo model potential[63] are also included. Good agreement between the present results and previous calculations of Shalenov *et al.*[48] and Chen *et al.*[13] over the wide range of plasma parameters indicates that the different choice of electron wavelength has a negligible effect on the ground state energies of the electron-ion subsystem. Large discrepancies only exist in the region where the ground state energy approaches zero, i.e., the critical bound region. In these loosely bound systems, large portions of electron probability densities are distributed into the far asymptotic distances, and the electron wave functions can be significantly different from the hydrogen-like ones (see, e.g., Fig. 3 in Ref. 68). The present GPS numerical calculations achieve full convergence in the critical

TABLE II. Ground state energies of the hydrogen atom in semiclassical dense plasmas under Eq. (6) with $k_i \neq 0$. Those places without data are due to either the nonexistence of bound states or being out of the valid range of the interaction potential (labeled by "–"). Energies are given in atomic units. Numbers in parentheses represent powers of ten.

	r_s								
θ	0.01	0.05	0.1	0.5	1	5	10	50	100
1000	−1.175 78(−1)	−2.872 93(−1)	−3.415 44(−1)	−4.239 27(−1)	−4.452 78(−1)	−4.749 55(−1)	−4.821 93(−1)	−4.919 82(−1)	−4.943 24(−1)
700	−7.739 15(−2)	−2.543 83(−1)	−3.152 20(−1)	−4.101 01(−1)	−4.351 22(−1)	−4.701 76(−1)	−4.787 73(−1)	−4.904 31(−1)	−4.932 27(−1)
500	−4.301 00(−2)	−2.203 71(−1)	−2.872 93(−1)	−3.949 68(−1)	−4.239 27(−1)	−4.648 57(−1)	−4.749 59(−1)	−4.886 99(−1)	−4.920 02(−1)
300	−6.199 27(−3)	−1.642 18(−1)	−2.391 41(−1)	−3.675 67(−1)	−4.034 36(−1)	−4.549 83(−1)	−4.678 56(−1)	−4.854 69(−1)	−4.897 20(−1)
100		−4.301 01(−2)	−1.175 78(−1)	−2.872 97(−1)	−3.415 54(−1)	−4.239 85(−1)	−4.453 87(−1)	−4.752 40(−1)	−4.825 35(−1)
70		−1.451 76(−2)	−7.739 23(−2)	−2.543 92(−1)	−3.152 41(−1)	−4.102 16(−1)	−4.353 33(−1)	−4.706 80(−1)	−4.793 58(−1)
50		−6.651 87(−4)	−4.301 09(−2)	−2.203 86(−1)	−2.873 30(−1)	−3.951 80(−1)	−4.243 10(−1)	−4.657 04(−1)	−4.759 12(−1)
30			−6.200 15(−3)	−1.642 52(−1)	−2.392 30(−1)	−3.680 97(−1)	−4.043 60(−1)	−4.567 82(−1)	−4.697 85(−1)
10				−4.313 47(−2)	−1.180 51(−1)	−2.905 52(−1)	−3.467 34(−1)	−4.315 09(−1)	−4.525 67(−1)
7				−1.464 75(−2)	−7.810 70(−2)	−2.598 84(−1)	−3.237 13(−1)	−4.213 66(−1)	–
5				−7.120 44(−4)	−4.394 68(−2)	−2.290 25(−1)	−3.002 92(−1)	–	–
3					−6.996 72(−3)	−1.799 08(−1)	−2.619 72(−1)	–	–

TABLE III. Same as Table II but for the potential in Eq. (6) with $k_i = 0$.

	r_s								
θ	0.01	0.05	0.1	0.5	1	5	10	50	100
1000	−1.964 08(−1)	−3.415 44(−1)	−3.836 92(−1)	−4.452 78(−1)	−4.608 29(−1)	−4.821 92(−1)	−4.873 59(−1)	−4.943 22(−1)	−4.959 84(−1)
700	−1.563 39(−1)	−3.152 20(−1)	−3.634 19(−1)	−4.351 22(−1)	−4.534 52(−1)	−4.787 72(−1)	−4.849 20(−1)	−4.932 23(−1)	−4.952 08(−1)
500	−1.175 78(−1)	−2.872 93(−1)	−3.415 44(−1)	−4.239 27(−1)	−4.452 78(−1)	−4.749 57(−1)	−4.821 97(−1)	−4.919 95(−1)	−4.943 43(−1)
300	−6.101 43(−2)	−2.391 41(−1)	−3.028 04(−1)	−4.034 36(−1)	−4.302 02(−1)	−4.678 50(−1)	−4.771 13(−1)	−4.897 06(−1)	−4.927 33(−1)
100		−1.175 78(−1)	−1.964 09(−1)	−3.415 49(−1)	−3.837 04(−1)	−4.453 39(−1)	−4.609 43(−1)	−4.824 85(−1)	−4.877 12(−1)
70		−7.739 19(−2)	−1.563 40(−1)	−3.152 31(−1)	−3.634 41(−1)	−4.352 42(−1)	−4.536 70(−1)	−4.792 93(−1)	−4.855 29(−1)
50		−4.301 05(−2)	−1.175 80(−1)	−2.873 12(−1)	−3.415 86(−1)	−4.241 52(−1)	−4.456 79(−1)	−4.758 41(−1)	−4.832 00(−1)
30		−6.199 71(−3)	−6.101 78(−2)	−2.391 86(−1)	−3.029 10(−1)	−4.040 08(−1)	−4.311 87(−1)	−4.697 71(−1)	−4.791 99(−1)
10				−1.178 22(−1)	−1.970 91(−1)	−3.453 47(−1)	−3.896 21(−1)	−4.541 05(−1)	−4.695 54(−1)
7				−7.776 43(−2)	−1.575 06(−1)	−3.219 08(−1)	−3.734 85(−1)	−4.488 20(−1)	–
5				−4.350 51(−2)	−1.194 22(−1)	−2.983 53(−1)	−3.576 46(−1)	–	–
3				−6.630 48(−3)	−6.420 58(−2)	−2.613 87(−1)	−3.336 86(−1)	–	–

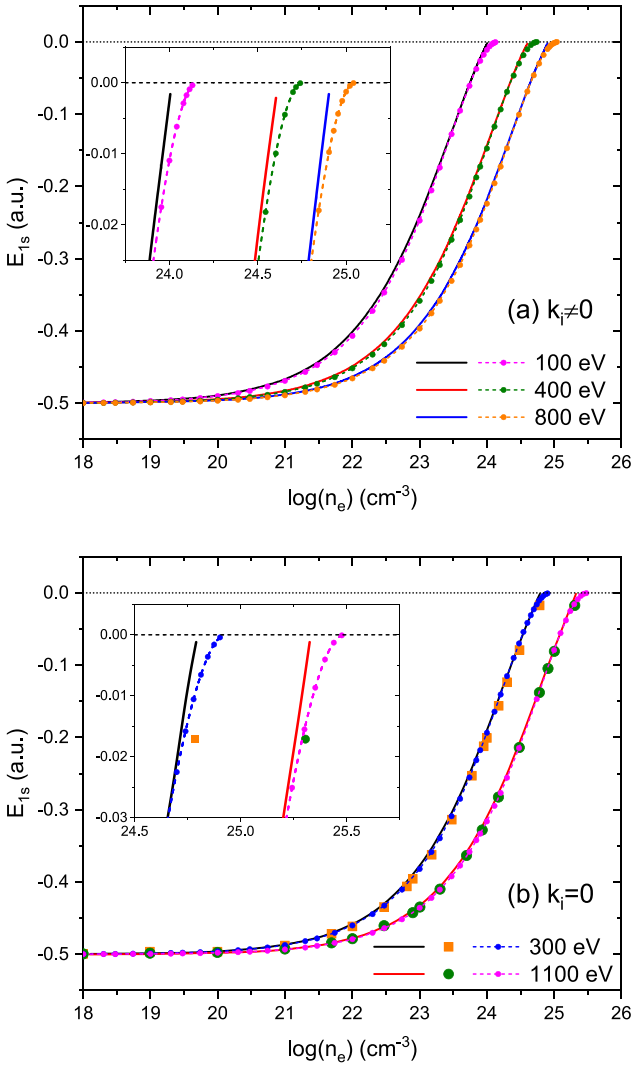

FIG. 2. Ground state energies of the H atom in semiclassical dense hydrogen plasmas. (a) Comparison of the energies under potential with $k_i \neq 0$ at $k_B T_e = 100$, 400, and 800 eV and $n_e = 10^{18}$ to 10^{26} cm^{-3}. (b) Comparison of the energies under potential with $k_i = 0$ at $k_B T_e = 300$ and 1100 eV and $n_e = 10^{18}$ to 10^{26} cm^{-3}. In both figures, solid lines represent the variational calculations of Shalenov *et al.*,[48] dashed–dotted lines are the present GPS numerical calculations, and solid dots are from Chen *et al.*[13] using the Stanton–Murillo model potential.[63] The insets in both figures show an enlarged view of the critical bound region.

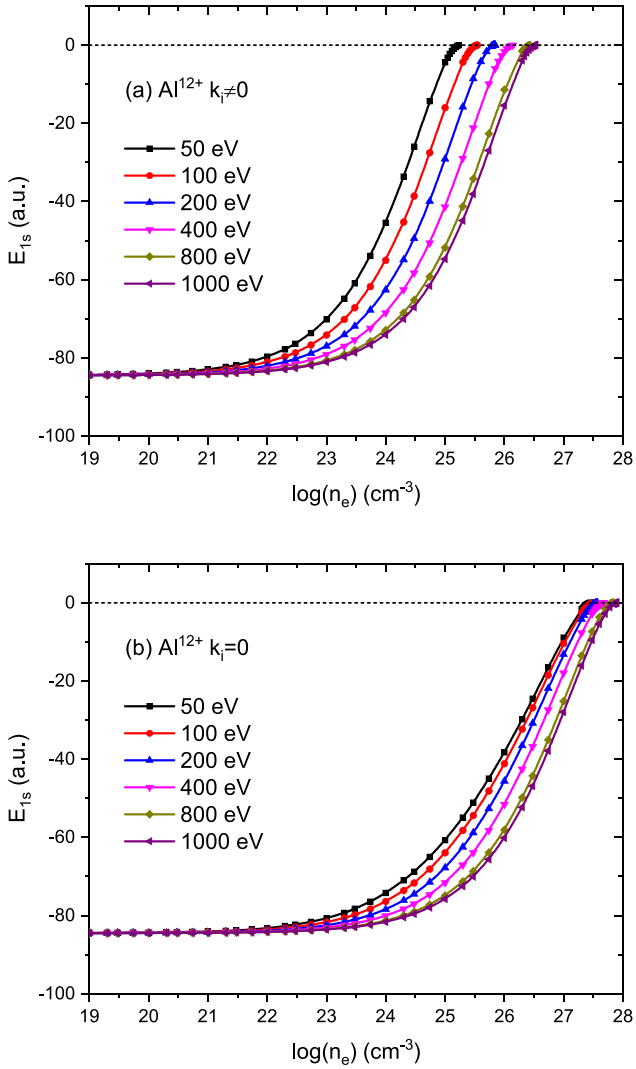

FIG. 3. Same as Fig. 2 but for the H-like Al ion ($Z = 13$) in semiclassical dense plasmas. (a) The ground state energies of Al^{12+} ion under the Ramazanov potential with $k_i \neq 0$ at $k_B T_e = 50$, 100, 200, 400, 800, and 1000 eV and $n_e = 10^{19}$ to 10^{28} cm^{-3}. (b) The ground state energies under the Ramazanov potential with $k_i = 0$.

bound region and are systematically lower than the predictions of Shalenov *et al.*[48] The single-parameter variational method utilizing hydrogenic wave functions employed by those authors probably loses its accuracy in the system critical bound limit.[71]

The comparison between Figs. 2(a) and 2(b) indicates that the inclusion of the ionic screening effect ($k_i \neq 0$) further reduces the binding energy of the electron-ion subsystem in plasmas, leading to a more loosely bound system. To take a clear view of the ionic screening effect in highly charged ions, we present in Fig. 3 the ground state energies of the H-like Al^{12+} ion ($Z = 13$) in the semiclassical dense plasmas,[72] where the thermodynamic equilibrium condition of $n_e = 13 n_i$ is employed in formulating k_e, k_i, and k_D. Results for the plasma temperatures of $k_B T_e = 50$, 100, 200, 400, 800, and 1000 eV and $n_e = 1 \times 10^{19}$ to 1×10^{28} cm^{-3} are shown in Figs. 3(a) and 3(b) for $k_i \neq 0$ and $k_i = 0$, respectively. It can be clearly observed that the ionic screening effect plays a more important role in heavier charged ions to decrease the system binding energies, especially in the dense plasma region where the bound state eventually merges into continuum. A systematic investigation of the variation of bound state energies for different charged ions is nevertheless beyond the scope of the present work. Additionally, we restrict our discussion on the semiclassical dense hydrogen plasmas and focus on the critical region where the system makes a bound-continuum phase transition.

B. Critical parameters and critical bound region

The critical bound-continuum transition of quantum systems has attracted long-term interest in past decades from both fundamental quantum mechanics and mathematical physics.[52–56] For example, the asymptotic behavior of bound states in the Debye–Hückel screened Coulomb potential has been extensively investigated in the literature by many authors, and the corresponding critical screening parameters have been determined to very high accuracy (see Ref. 68 and references therein). The mathematical foundation of the quantum phase transition in the critical region was built by Klaus and Simon[73] and Kais and Serra.[53] Those authors have shown that for a short-range potential with a linear parameter μ, i.e., the Hamiltonian is given by $H = T + \mu V$, the leading order of eigenenergies of the s-wave bound states near the transition threshold follows the quadratic law:

$$E(\mu) \propto (\mu - \mu_c)^2, \tag{20}$$

where μ_c is the critical parameter. In view of the variation of the ground state energies shown in Fig. 2, it is of great interest to investigate the corresponding asymptotic behavior in the transition region.

Figure 4 displays the asymptotic behavior of the ground state energies of the electron-ion subsystem in semiclassical dense plasmas at $r_s = 0.1$ near the critical degeneracy parameter of θ_c, for both $k_i \neq 0$ and $k_i = 0$. The values of θ_c were calculated using the combination of the GPS numerical method with Brent's minimization algorithm,[74] and the computational details are available in Ref. 68. In general, the critical parameters can be efficiently determined with a similarly high accuracy as the bound state energies of the system. For $r_s = 0.1$, it is obtained that $\theta_c = 22.983\,028\,913\ldots$ and $11.490\,596\,239\ldots$ for $k_i \neq 0$ and $k_i = 0$, respectively. From Fig. 4, it can be interestingly found that the ground state energies of the system under the model potential Eq. (6) follow exactly the same quadratic law as Eq. (20). The power-law fittings of the numerical calculations yield

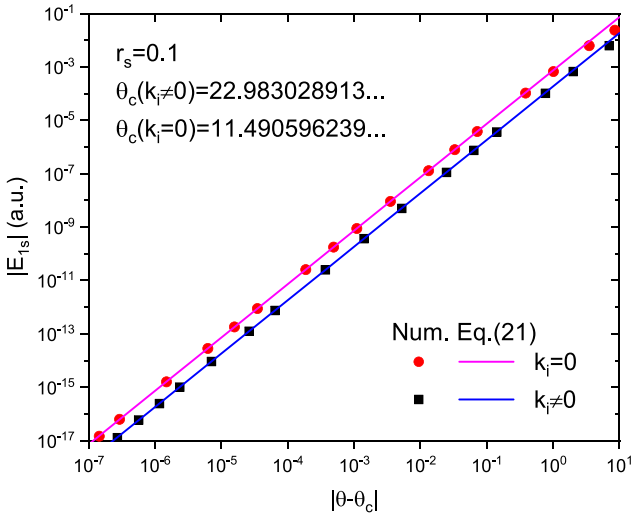

FIG. 4. Asymptotic behavior of the ground state energies of the hydrogen atom in semiclassical dense plasmas at $r_s = 0.1$ near the critical bound region of θ. The critical electron degeneracy parameters θ_c are calculated using the GPS method. Dots are the present numerical calculations and solid lines are the power-law fittings based on Eq. (21).

$$\begin{aligned} E_{1s} &\approx -1.84 \times 10^{-4}(\theta - \theta_c)^2 \quad \text{for } k_i \neq 0, \\ E_{1s} &\approx -7.37 \times 10^{-4}(\theta - \theta_c)^2 \quad \text{for } k_i = 0. \end{aligned} \tag{21}$$

Although the dependence of Eq. (6) upon the parameter θ is not as straightforward as a linear parameter, we find that a similar quadratic law applies to a wide variety of short-range potentials.[70] Variation of the ground state energies of the electron-ion subsystem at fixed values of θ with varying electron density parameter n_e also follow the quadratic law (the results are not shown here for simplicity). These findings explain very well the asymptotic behavior of the ground state energies shown in the insets of Fig. 2.

The critical degeneracy parameters of θ_c for the ground state of the electron-ion subsystem in semiclassical dense plasmas are summarized in Table IV for the density parameters r_s ranging from 10^{-2} to 10, within the potential valid range. It was found that θ_c decreases monotonically with increasing r_s and the values of $k_i = 0$ are always smaller than those of $k_i \neq 0$. This indicates that inclusion of the ionic screening effect in the model potential pushes the critical bound region into a stronger non-degenerate (classical) region. The critical degeneracy parameters for $r_s \geq 5$ ($\theta_c \leq 0.28$) are also provided in the table for completeness, although we must keep in mind that they are in the degenerate quantum plasma region.

TABLE IV. Critical degeneracy parameters of θ_c for the ground state of the electron-ion subsystem in semiclassical dense plasmas under Eq. (6) at some selected values of r_s.

r_s	θ_c ($k_i \neq 0$)	θ_c ($k_i = 0$)
0.01	229.836 406	114.918 194
0.015	153.224 261	76.612 109 9
0.02	114.918 181	57.459 054 1
0.03	76.612 082 3	38.305 958 4
0.05	45.967 129 3	22.983 334 9
0.07	32.833 473 0	16.416 286 4
0.1	22.983 028 9	11.490 596 2
0.15	15.321 050 8	7.658 462 40
0.2	11.489 376 8	5.741 030 24
0.3	7.655 745 28	3.819 715 95
0.5	4.581 884 50	2.269 023 25
0.7	3.255 405 26	1.586 737 62
0.85	2.664 285 64	1.274 149 67
1	2.245 903 10	1.046 014 65
1.15	1.932 667 54	0.868 816 87
1.4	1.552 935 57	
1.5	1.434 489 37	
1.6	1.329 928 19	
5	0.282 198 73	
6	0.222 218 80	
7	0.183 439 32	
8	0.156 424 05	
10	0.121 258 03	
12	0.099 299 44	
15	0.078 317 48	

A systematic view of the critical bound-continuum transition in the present system is given in Fig. 5. Figure 5(a) is displayed in terms of the dimensionless parameters r_s and θ, while Fig. 5(b) is the transformed diagram depending upon the electron density n_e and temperature k_BT_e. Both figures are shown in the logarithmic scale. Also included in these figures are the $\theta = 1$ line which separates the classical and quantum plasmas and the $\Gamma = 1$ line dividing the weakly and strongly coupled plasmas. In Fig. 5(a), the electron-ion bound region is located in the upper right part of the figure, which generally lies in the classical and weakly coupled plasma region. This is consistent with our previous approximation of the electron thermal de Broglie wavelength that the electron

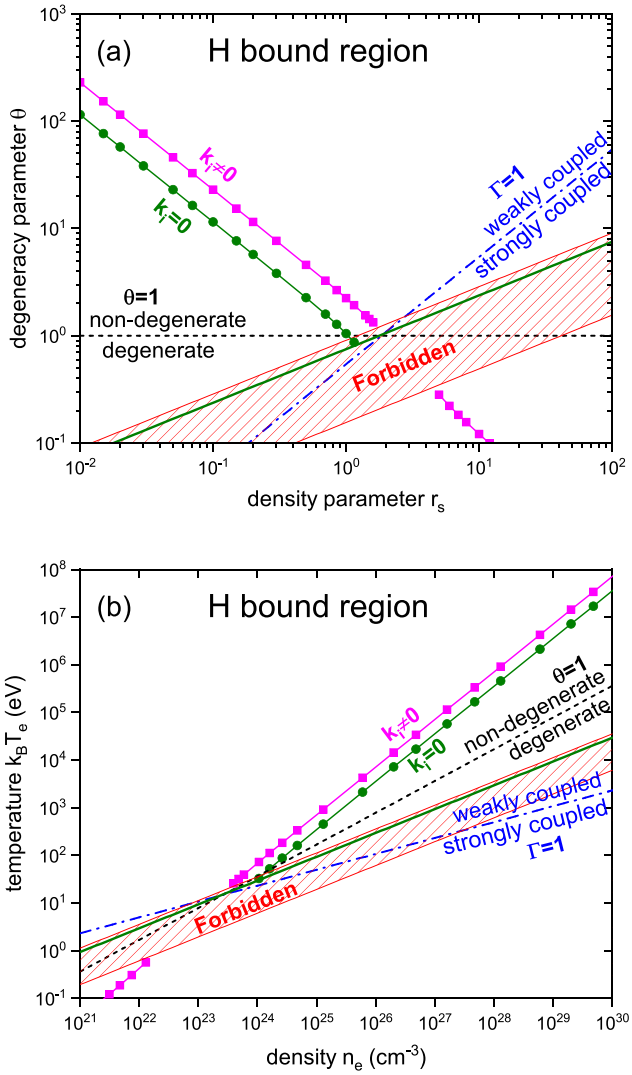

FIG. 5. Diagrams of the critical bound region of the electron-ion subsystem in semiclassical dense plasmas. (a) Critical lines in terms of dimensionless parameters r_s and θ. (b) Critical lines in terms of electron density n_e and plasma temperature k_BT_e. In both figures, the $\theta = 1$ and $\Gamma = 1$ lines and the forbidden region of effective potential with $k_i \neq 0$ are included to guide the eyes. The system bound region lies above the critical transition lines.

quantum degenerate and exchange-correlation effects are not important in the calculation of bound state energies in these plasmas. The critical transition line for $k_i \neq 0$ is broken by the forbidden region, while the line for $k_i = 0$ only exists in the upper part of the figure and lies slightly lower than the $k_i \neq 0$ line. Figure 5(b) is obtained by transforming Fig. 5(a) via the variable transformations in Eqs. (11) and (12). It can be clearly observed that bound states exist in comparably low electron densities and relatively high temperatures.

We further show in Fig. 6 the contour plots of the ground state energies in terms of variables r_s, θ and n_e, k_BT_e, for both $k_i \neq 0$ and $k_i = 0$. In all situations, the contour lines generally follow a similar slope as the critical transition lines, except near the forbidden region where the contour lines are slightly distorted. Figures 6(b) and 6(d) are obtained via the variable transformations from Figs. 6(a) and 6(c), respectively, and therefore, some contour lines near the critical transition region may appear slightly distorted. A distinct feature that can be observed from Figs. 6(b) and 6(d) is that the bound state energies change rapidly when the plasmas approach the critical transition line. In other regions, the electrons are either well-bounded by the ions or, on the contrary, move as free particles. These figures provide a systematic view of and fast access to the distribution of the electron-ion ground state energies in semiclassical dense hydrogen plasmas and potentially serve as a useful tool in diagnosing plasma parameters and modeling the electron-ion collisional dynamics.

C. Oscillator strengths and polarizabilities

The transition and polarization quantities of atomic systems embedded in plasmas play a crucial role in understanding the macroscopic optical properties of plasmas and the nonlinear response of micro electron-ion subsystems under the influence of external electric field.[7–11,75–77] In this section, we focus on the dipole transitions and static dipole polarizabilities of the hydrogen atom in its ground state under different plasma conditions, with special attention paid to their asymptotic behavior in the critical bound region. By employing the sum-over-states method within the framework of standard perturbation theory,[77,78] the static dipole polarizability for an atom in the initial i state is given by

$$\alpha_i = \sum_f \frac{\bar{o}_{fi}}{(\Delta E_{fi})^2}, \tag{22}$$

where $\Delta E_{fi} = E_f - E_i$ represents the transition energy from the initial i to the final f states and $\bar{o}_{fi}$ refers to the mean dipole transition oscillator strength that has been averaged over the initial-state orientation degeneracy and summed over the final-state degeneracy,[79]

$$\bar{o}_{fi} = \frac{8\pi}{3}\frac{\Delta E_{fi}}{2l_i+1}\sum_{m_i}\sum_{m_f}|\langle n_f l_f m_f|rY_{1q}(\hat{r})|n_i l_i m_i\rangle|^2. \tag{23}$$

The summation in Eq. (22) ideally extends over all possible final states which include both bound and continuum spectra of the system in a given symmetry.

With the help of the Wigner–Eckart theorem and the selection rule of the 3j symbol, the dipole transition from an initial state in the s-wave symmetry ensures that only p-wave states are allowed in the final states ($\Delta l = \pm 1$). It is then readily obtained that

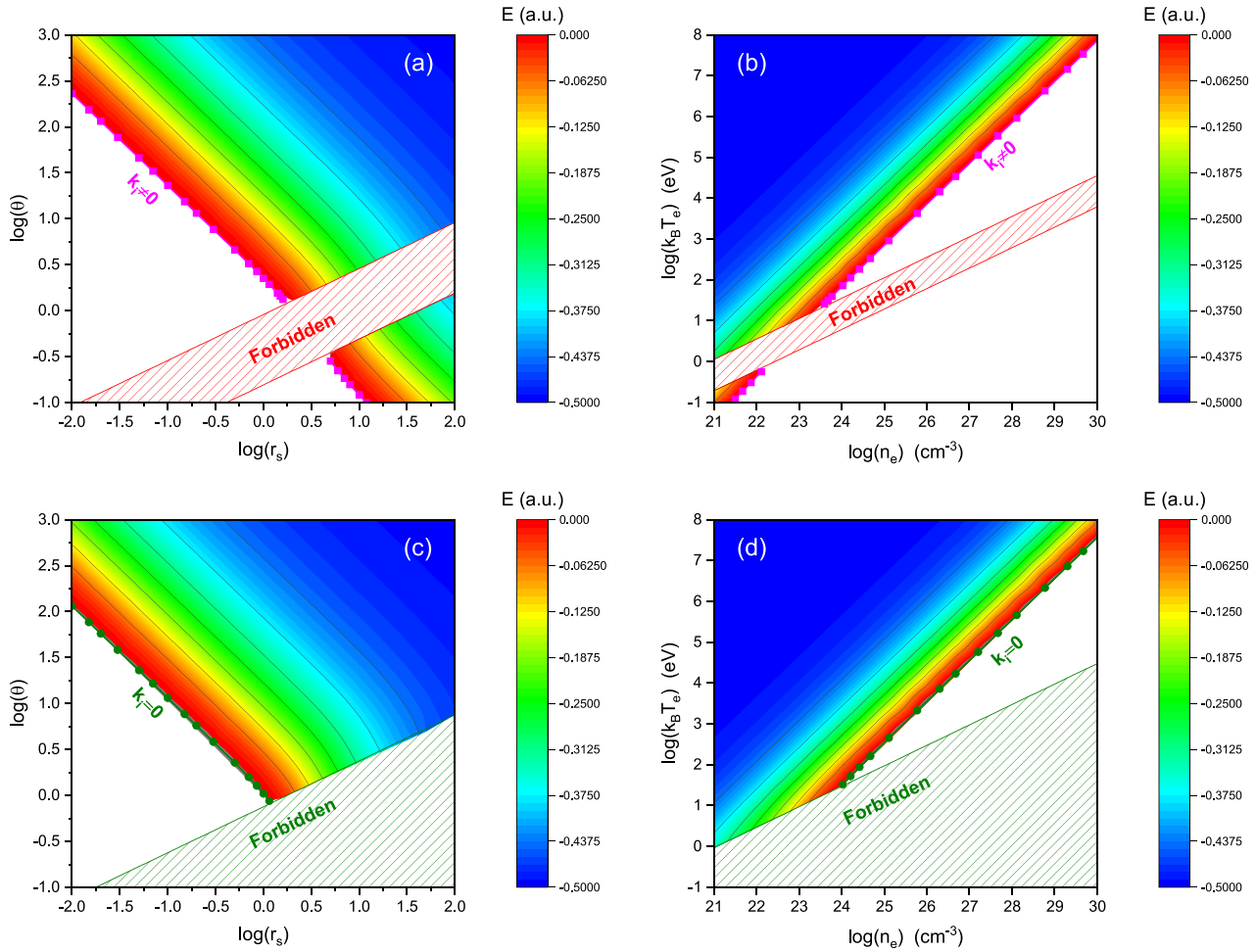

FIG. 6. Contour plots of the ground state energies of the electron-ion subsystem in semiclassical dense plasmas. (a) Energy distribution with $k_i \neq 0$ given in terms of r_s and θ. (b) Same as (a) but in terms of n_e and $k_B T_e$. (c) Energy distribution with $k_i = 0$ given in terms of r_s and θ. (d) Same as (c) but in terms of n_e and $k_B T_e$.

$$\bar{o}_{ps} = 2\Delta E_{ps} |\langle r \rangle_s^p|^2 \begin{Bmatrix} 1 & 1 & 0 \\ 0 & 0 & 0 \end{Bmatrix}^2 = \frac{2}{3} \Delta E_{ps} |\langle r \rangle_s^p|^2, \tag{24}$$

where

$$\langle r \rangle_{n_i l_i}^{n_f l_f} = \int_0^\infty \psi_{n_f l_f}(r) r \psi_{n_i l_i}(r) dr, \tag{25}$$

defines the radial dipole transition matrix element. In the present work, all system radial wave functions $\psi_{nl}(r)$ were obtained by solving Eq. (18) using the GPS numerical method mentioned in Sec. II D. The computational convergence can be estimated by checking the normalization condition (Thomas–Reiche–Kuhn sum rule[79]) of the dipole transition oscillator strength, i.e., $S = \sum_f \bar{o}_{fi} \equiv 1$ for the one-electron systems.

In Fig. 7(a), we show the variation of the oscillator strength for the strongest $1s \rightarrow 2p$ dipole transition of the hydrogen atom at some selected values of plasma temperatures $k_B T_e$ same as those in Fig. 2(a), for both $k_i \neq 0$ and $k_i = 0$. At extremely low densities where the plasma screening effect is negligible, all oscillator strengths approach the analytical free-atom value of $2^{13}/3^9 = 0.416\,196\,7$. With gradually increasing the plasma density, the oscillator strength decreases monotonically to zero, which represents a continuous lowering of the radiative transition probability from the ground state to the $2p$ excited state. Such a trend can be understood from Eq. (24) that the oscillator strength is primarily determined by the radial transition matrix element of Eq. (25). The plasma screening potential has a stronger effect of expanding the $2p$ wave function in the configuration space than that of the ground state and, as a result, the "overlap" between these two states decreases with gradually enhancing the screening effect (i.e., increasing n_e). The comparison between Figs. 2(a) and 7(a) reveals an interesting phenomenon that the $1s \rightarrow 2p$ transition oscillator strength (actually for all $1s \rightarrow np$ transitions) becomes zero much faster than the ground state energy. This is because the critical plasma density for the $2p$ state is much smaller than that of the ground state under the same plasma temperature [e.g., at $k_B T_e = 100$ eV the critical densities $\log(n_e)$ for the $1s$ and $2p$ states are 24.15 and 22.68 cm^{-3}, respectively]. The similar phenomenon has also been observed in the Debye–Hückel screened Coulomb potential.[11] When the $2p$ state is absorbed

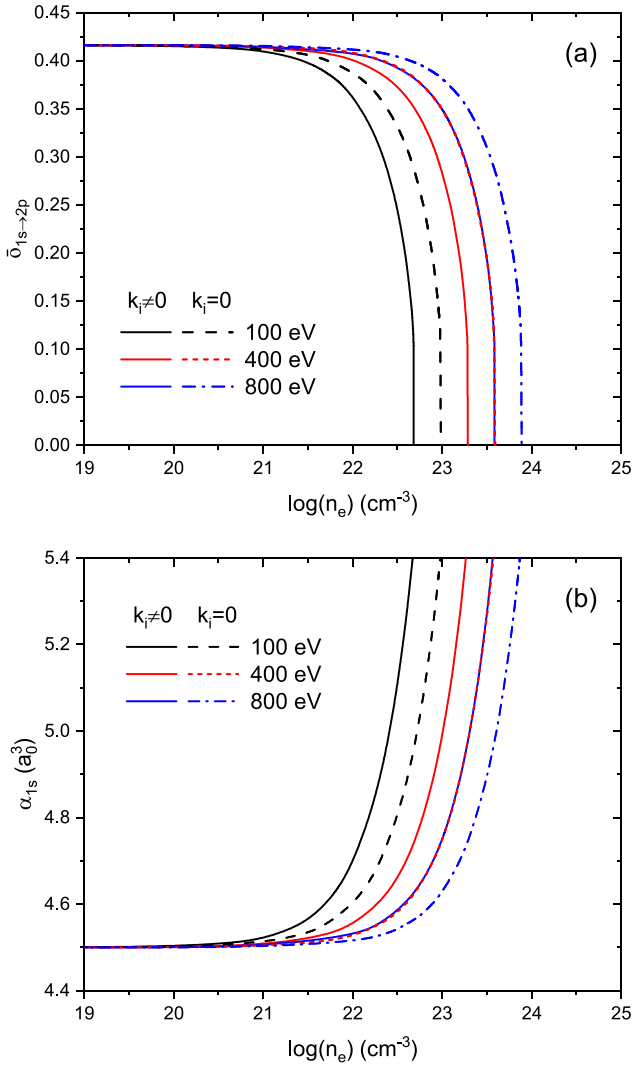

FIG. 7. (a) Oscillator strength for the $1s \to 2p$ transition at plasma temperatures $k_B T_e = 100$, 400, and 800 eV for both $k_i \neq 0$ and $k_i = 0$. (b) Same as (a) but for the dipole polarizability of the ground state of the hydrogen atom in semiclassical dense plasmas. The accidental overlap between curves of $k_B T_e = 800$ eV ($k_i \neq 0$) and $k_B T_e = 400$ eV ($k_i = 0$) is due to the similar critical screening parameters under these plasma parameters for both the 1*s* and 2*p* states.

into the continuum, the individual $1s \to 2p$ transition loses its physical significance and only the summation of an infinite number of continuum spectra contributes to the normalization condition of the oscillator strength $S \equiv 1$.

The shift of the system eigenenergies under a weak external electric field up to the second-order correction is determined by

$$E_{nl}(F) = E_{nl}^0 - \frac{\alpha_{nl}}{2} F^2 - \ldots, \tag{26}$$

where E_{nl}^0 is the system eigenenergy without the electric field [solution of Eq. (18)] and F is the strength of electric field. It should be kept in mind that the first-order energy correction is exactly zero due to the odd parity of the dipole interaction operator.[77] The static polarizability α_{nl} can be efficiently calculated through the summation of oscillator strengths via Eq. (22). In Fig. 7(b), the variation of the ground state dipole polarizability of the hydrogen atom in semiclassical dense plasmas is displayed as a function of the plasma density, at fixed values of plasma temperatures. The fast increase in dipole polarizability at large densities indicates that the system ground state wave function can be easily distorted by the external electric field, resulting in a large energy shift. This is consistent with the monotonic increase in the ground state energies (E_{1s}^0) shown in Fig. 2, i.e., the electron-ion subsystems in the semiclassical dense plasmas become more loosely bound in stronger screening conditions. The opposite behavior of the oscillator strengths in Fig. 7(a) and polarizabilities in Fig. 7(b) further manifests that the contribution of individual discrete bound states in calculating polarizability becomes increasingly small (and eventually disappears) at large plasma densities.

From Eqs. (20) and (21), we know that near the system critical bound limit, the ground state energy (without electric field) approaches zero by following a quadratic law. It is therefore of great interest to investigate the asymptotic behavior of the polarizability when the system approaches the bound limit. Figure 8 displays the variation of the ground state dipole polarizability for the hydrogen atom in semiclassical dense plasmas at $r_s = 0.1$ (for both $k_i \neq 0$ and $k_i = 0$) near corresponding critical degeneracy parameters θ_c. They are shown in a similar logarithmic scale as those of Fig. 4. Our numerical calculations based on the GPS method are denoted by dots. The power-law fittings (denoted by solid lines) yield

$$\begin{aligned} \alpha_{1s} &\approx 1.84 \times 10^6 (\theta - \theta_c)^{-4} \quad \text{for } k_i \neq 0, \\ \alpha_{1s} &\approx 1.15 \times 10^5 (\theta - \theta_c)^{-4} \quad \text{for } k_i = 0. \end{aligned} \tag{27}$$

The fast increase in dipole polarizability, in contrast to the fast decrease in the field-free energy (in Fig. 4), represents the failure of the second-order correction formula in Eq. (26) at relatively large values of field

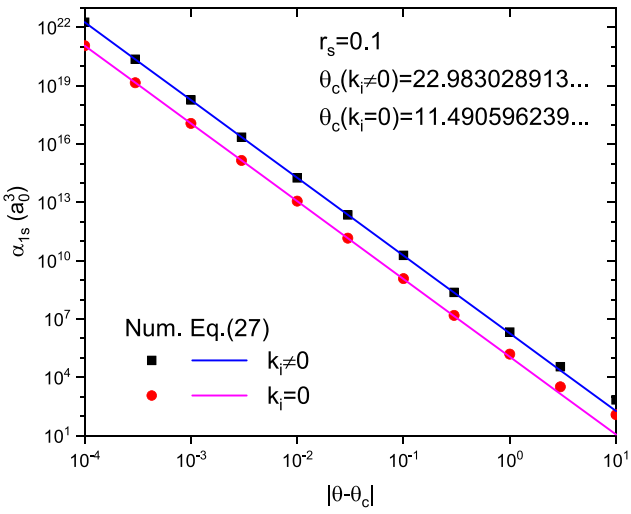

FIG. 8. Asymptotic behavior of the ground state polarizabilities of the hydrogen atom in semiclassical dense plasmas at $r_s = 0.1$ near the critical bound region of θ. Dots are the present numerical calculations and solid lines are the power-law fittings based on Eq. (27).

strength F. When a system is nearing its bound-continuum transition limit, the loosely bound character of the system wave function manifests a highly nonlinear response under the distortion of the external electric field, indicating the failure of finite-order perturbation methods in approximating the system. From the discussion in Sec. III B, we may conjecture that for a quantum system described by the Hamiltonian $H = T + \mu V$, where V is a short-range potential and μ the linear parameter, the dipole polarizability of the s-wave bound states near the transition threshold probably follows an inverse biquadratic law:[12]

$$\alpha(\mu) \propto (\mu - \mu_c)^{-4}, \tag{28}$$

where μ_c is the critical parameter.

For a systematic view of the variation of dipole polarizability for the plasma-embedded hydrogen atom over a wide range of plasma parameters, we show in Table V the present numerical calculations at a large collection of plasma density parameter r_s and electron degeneracy parameter θ. Full computational convergence is achieved by gradually increasing the dimension of discretization in the GPS method as well as by estimating the normalization condition of the oscillator strengths. All numerical values are expected to be accurate up to their last reported digits. In the top-right section of the table, where the non-degenerate classical plasma has extremely low densities and high temperatures, the embedded electron-ion subsystems can be well-approximated by free atoms and the dipole polarizabilities are close to the analytical value of 9/2 for the hydrogen atom.[79] The magnitude of polarizability increases monotonically with either increasing the plasma density or decreasing the temperature (more specifically, increasing the electron quantum degenerate effect). Especially when the system approaches the critical bound limit, the polarizability increases by several orders of magnitude. A similar table but for the plasma potential with $k_i = 0$, i.e., without considering the screening effect of ions, is given in Table VI. All numerical values shown in Table VI are systematically smaller than those in Table V at the same plasma parameters. The comparison between these two tables guides us to the same conclusion as in the comparison between Tables II and III that the more tightly bound of the system gives rise to a smaller value of polarizability.

D. Limitations and perspectives

The existence of multiply charged ions in real plasmas makes the simulation of multi-electron systems in semiclassical dense plasmas more valuable (and also more challenging) than that of the simplest one-electron system investigated in the present work. On the other hand, the investigation of multi-electron systems and the corresponding collision and radiation processes in different screening potentials would provide generally a comprehensive view of the structural information and dynamic properties of atomic and ionic pieces in different plasma environments. In this regard, we would like to mention that there exist in the literature a large number of research focused on the multi-electron systems in plasmas utilizing different microscopic model potentials. Those are, for example, the two-electron He atom and He-like charged ions,[80–90] the exotic systems including positron,[91–95] and the more complex multi-electron atoms and ions described either by model potentials or by explicit treatment of full electronic interactions.[96–104] On the other hand, various electron-atom, positron-atom, and ion-atom scattering processes as well as the nonlinear response of atoms irradiated by intense laser field[105–109] also attract considerable interest in the literature in recent years (see, e.g., Ref. 9 for a thorough review of quantum collision dynamics in plasmas). To the best of our knowledge, most of these research were performed under the Debye–Hückel[2,17] and ion-sphere[18] model potentials for the weakly and strongly coupled plasmas, respectively, and the modified exponential-cosine Debye-Hückel potential[26] designed specially for the quantum dense plasmas.

For the semiclassical dense plasmas considered in this work, the model potentials developed by Ramazanov *et al.*[29–32] provide a systematic and consistent description of the electron–electron, ion–ion, and electron-ion effective interactions between pairs of charged particles based on the momentum-space dielectric function in linear response approximation. The application of these potentials to the structure

TABLE V. Dipole polarizabilities of the hydrogen atom in semiclassical dense plasmas under Eq. (6) with $k_i \neq 0$. Those places without data are due to either the nonexistence of bound states or being out of the valid range of the interaction potential (labeled by "–"). Polarizability has the dimension of volume in atomic units, and therefore numerical results are given in units of a_0^3. Numbers in parentheses represent powers of ten.

	r_s								
θ	0.01	0.05	0.1	0.5	1	5	10	50	100
1000	1.481 496(1)	5.781 638	5.132 416	4.632 059	4.567 502	4.514 011	4.507 062	4.501 360	4.500 629
700	2.622 327(1)	6.384 188	5.404 979	4.686 410	4.595 370	4.519 875	4.510 023	4.501 906	4.500 870
500	6.449 963(1)	7.276 184	5.781 637	4.758 122	4.632 050	4.527 611	4.513 930	4.502 611	4.501 180
300	2.013 675(3)	9.897 230	6.742 297	4.924 177	4.716 342	4.545 385	4.522 891	4.504 181	4.501 863
100		6.449 929(1)	1.481 485(1)	5.781 466	5.132 121	4.630 863	4.565 513	4.511 179	4.504 911
70		4.177 875(2)	2.622 281(1)	6.383 793	5.404 337	4.684 007	4.591 561	4.515 264	4.506 717
50		1.509 306(5)	6.449 690(1)	7.275 274	5.780 274	4.753 494	4.625 094	4.520 418	4.509 026
30			2.013 129(3)	9.893 550	6.737 759	4.911 707	4.699 354	4.531 623	4.514 151
10				6.416 448(1)	1.471 065(1)	5.675 873	5.025 690	4.580 583	4.537 667
7				4.108 972(2)	2.580 072(1)	6.169 052	5.215 090	4.609 522	–
5				1.320 043(5)	6.205 119(1)	6.847 198	5.455 880	–	–
3					1.598 633(3)	8.581 888	5.997 769	–	–

TABLE VI. Same as Table V but for the potential in Eq. (6) with $k_j = 0$.

	r_s								
θ	0.01	0.05	0.1	0.5	1	5	10	50	100
1000	8.158 831	5.132 417	4.820 499	4.567 504	4.534 392	4.507 074	4.503 547	4.500 643	4.500 269
700	1.046 754(1)	5.404 979	4.953 828	4.595 373	4.548 678	4.510 047	4.505 034	4.500 885	4.500 357
500	1.481 496(1)	5.781 637	5.132 416	4.632 055	4.567 495	4.513 974	4.506 992	4.501 187	4.500 463
300	3.729 008(1)	6.742 299	5.559 826	4.716 357	4.610 688	4.523 007	4.511 471	4.501 823	4.500 674
100		1.481 491(1)	8.158 778	5.132 268	4.820 225	4.566 328	4.532 421	4.504 245	4.501 396
70		2.622 304(1)	1.046 739(1)	5.404 656	4.953 250	4.593 027	4.544 915	4.505 443	4.501 726
50		6.449 826(1)	1.481 452(1)	5.780 951	5.131 238	4.627 576	4.560 653	4.506 793	4.502 085
30		2.013 402(3)	3.728 625(1)	6.740 002	5.556 240	4.704 521	4.594 141	4.509 266	4.502 710
10				1.476 098(1)	8.108 722	5.040 617	4.720 904	4.515 988	4.504 246
7				2.600 143(1)	1.033 131(1)	5.228 329	4.781 090	4.518 323	–
5				6.318 614(1)	1.441 615(1)	5.454 581	4.845 818	–	–
3				1.771 168(3)	3.406 775(1)	5.904 670	4.954 421	–	–

calculations of multi-electron systems and the large variety of collision processes would be of great interest and also of practical importance for the simulation of fundamental atomic processes in plasmas and the diagnosis of plasma parameters. It is worth mentioning that in calculating the multi-electron atoms in semiclassical dense plasmas, the original Coulomb potential between electrons should be substituted by the electron–electron effective interaction potential given by Eq. (8) of Ref. 32. The similar substitution applies in the investigation of electron- or positron-atom scattering in the semiclassical dense plasmas. On the other hand, the ion–ion effective interaction potential given by Eq. (9) of Ref. 32 would probably exhibit its importance in modeling the plasma-screened molecular systems (e.g., the H_2 molecule and H_2^+ molecular ion[110–113]) and the ion-atom scattering processes.[9] The present work which focuses only on the structure properties of the simplest H atom represents a preliminary attempt to such an effort.

IV. CONCLUSION

In this work, we investigated the bound state energies and critical bound region of the electron-ion subsystem in semiclassical dense hydrogen plasmas. The effective interaction between charged particles is represented by the Ramazanov model potential, which takes into account both the quantum effects of diffraction and symmetry between colliding particles and the screening effect of the plasma environment. Accurate ground state energies, either with or without considering the ionic screening effect, are obtained by numerically solving the Schrödinger equation using the GPS method. The present results are compared with previous calculations based on a different choice of electron wavelength. Good agreement of the potential energy curves and ground state energies indicates that in the system bound region, the electron quantum degeneracy and exchange-correlation effects do not play significant roles. We further calculated the critical plasma parameters where the bound-continuum transition occurs and found that the ground state energies follow a quadratic law in the critical bound region. The ground state energies of the electron-ion subsystem and corresponding static dipole polarizabilities were reported for a wide range of plasma parameters where the effective potential is valid. Investigation of the critical stability and asymptotic behavior of physical quantities of multi-electron-ion subsystems, especially the helium-like atoms,[114–117] in semiclassical or quantum dense plasmas would be of great interest in the future study.

Extension of the present work to the potential forbidden region is worth investigating in the future by employing the modified effective interaction potential developed by Ramazanov *et al.*[32] By removing the imaginary unit, the new potential takes a complicated form containing oscillating terms in the analytical expression. Accurate calculation of the system bound state energies and other physical quantities, however, need more careful examination of the computational convergence. Another more practical way is to use the alternative definition of the electron wavelength employed by Kodanova *et al.*[42] and Shalenov *et al.*[48] Such a choice extends the valid range of the potential into the deep degenerate quantum plasma region and is of particular interest in our future work.

ACKNOWLEDGMENTS

This work was supported by the National Key Research and Development Program of China (Grant No. 2022YFE0134200), the National Natural Science Foundation of China (Grant No. 12174147), and the Natural Science Foundation of Jilin Province, China (Grant No. 20220101016JC).

AUTHOR DECLARATIONS

Conflict of Interest

The authors have no conflicts to disclose.

Author Contributions

Tong Yan: Data curation (equal); Writing – original draft (equal). **Li Guang Jiao:** Funding acquisition (equal); Project administration (equal); Writing – original draft (equal). **Aihua Liu:** Funding acquisition (equal); Methodology (equal). **Yuan Cheng Wang:** Formal analysis (equal); Validation (equal). **H. E. Montgomery, Jr.:** Investigation (equal); Writing – review & editing (equal). **Yew Kam Ho:** Conceptualization (equal); Writing – review & editing (equal).

Stephan Fritzsche: Resources (equal); Writing – review & editing (equal).

DATA AVAILABILITY

The data that support the findings of this study are available within the article.

REFERENCES

[1]D. Salzman, *Atomic Physics in Hot Plasmas* (Oxford University Press, Oxford, 1998).
[2]J. Weisheit and M. Murillo, "Atoms in dense plasmas," in *Springer Handbook of Atomic, Molecular, and Optical Physics*, edited by G. Drake (Springer New York, New York, NY, 2006), Chap. 86, p. 1303.
[3]J. Bauche, C. Bauche-Arnoult, and O. Peyrusse, *Atomic Properties in Hot Plasmas: From Levels to Superconfigurations* (Springer International Publishing, Cham, 2015).
[4]Y.-D. Jung, Phys. Plasmas **10**, 502 (2003).
[5]B. Saha and S. Fritzsche, J. Phys. B **40**, 259 (2007).
[6]A. N. Sil, S. Canuto, and P. K. Mukherjee, Adv. Quantum Chem. **58**, 115 (2009).
[7]Y. Y. Qi, Y. Wu, J. G. Wang, and Y. Z. Qu, Phys. Plasmas **16**, 023502 (2009).
[8]A. Bhattacharya, M. Z. M. Kamali, A. Ghoshal, and K. Ratnavelu, Phys. Plasmas **22**, 023512 (2015).
[9]R. K. Janev, S. B. Zhang, and J. G. Wang, Matter Radiat. Extrem. **1**, 237 (2016).
[10]G. P. Zhao, Y. Y. Qi, L. Liu, J. G. Wang, and R. K. Janev, Phys. Plasmas **26**, 063509 (2019).
[11]L. Zhu, Y. Y. He, L. G. Jiao, Y. C. Wang, and Y. K. Ho, Phys. Plasmas **27**, 072101 (2020).
[12]L. G. Jiao, Y. Y. He, Y. Z. Zhang, and Y. K. Ho, J. Phys. B **54**, 065005 (2021).
[13]Z.-B. Chen, Y.-Y. Qi, H.-Y. Sun, G.-P. Zhao, and P.-F. Liu, Phys. Plasmas **27**, 072105 (2020).
[14]Z.-B. Chen, P.-F. Liu, H.-Y. Sun, Y.-Y. Qi, G.-P. Zhao, X.-Z. Shen, L.-G. Jiao, K. Ma, K. Wang, and X.-D. Li, Int. J. Quantum Chem. **122**, e26842 (2022).
[15]S. Mondal, S. K. Nayek, and J. K. Saha, Eur. Phys. J. Plus **137**, 373 (2022).
[16]Z.-B. Chen, Phys. Plasmas **29**, 102102 (2022).
[17]P. Debye and E. Hückel, Z. Phys. **24**, 185 (1923).
[18]S. Ichimaru, Rev. Mod. Phys. **54**, 1017 (1982).
[19]"There exists in the literature an alternative definition of the quantum degenerate parameter which is given by the ratio of electron fermi energy to the thermal energy.[2]"
[20]P. K. Shukla and B. Eliasson, Phys. Rev. Lett. **108**, 165007 (2012).
[21]P. K. Shukla and B. Eliasson, Phys. Rev. Lett. **108**, 219902 (2012).
[22]P. K. Shukla and B. Eliasson, Phys. Rev. Lett. **109**, 019901 (2012).
[23]M. Akbari-Moghanjoughi, Phys. Plasmas **22**, 022103 (2015).
[24]B. Eliasson and M. Akbari-Moghanjoughi, Phys. Lett. A **380**, 2518 (2016).
[25]M. Akbari-Moghanjoughi, A. Abdikian, and A. Phirouznia, Phys. Plasmas **27**, 042107 (2020).
[26]P. K. Shukla and B. Eliasson, Phys. Lett. A **372**, 2897 (2008).
[27]M. Bonitz, T. Dornheim, Z. A. Moldabekov, S. Zhang, P. Hamann, H. Kählert, A. Filinov, K. Ramakrishna, and J. Vorberger, Phys. Plasmas **27**, 042710 (2020).
[28]D. Kang, Y. Hou, Q. Zeng, and J. Dai, Matter Radiat. Extrem. **5**, 055401 (2020).
[29]T. S. Ramazanov and K. N. Dzhumagulova, Phys. Plasmas **9**, 3758 (2002).
[30]T. S. Ramazanov, K. N. Dzhumagulova, Y. A. Omarbakiyeva, and G. Röpke, J. Phys. A **39**, 4369 (2006).
[31]T. S. Ramazanov, K. N. Dzhumagulova, and M. T. Gabdullin, Phys. Plasmas **17**, 042703 (2010).
[32]T. S. Ramazanov, Z. A. Moldabekov, and M. T. Gabdullin, Phys. Rev. E **92**, 023104 (2015).
[33]C. Deutsch, Phys. Lett. A **60**, 317 (1977).
[34]K. N. Dzhumagulova, E. O. Shalenov, T. S. Ramazanov, and G. L. Gabdullina, Contrib. Plasma Phys. **55**, 230 (2015).
[35]T. S. Ramazanov, S. M. Amirov, and Z. A. Moldabekov, Contrib. Plasma Phys. **58**, 155 (2018).
[36]K. N. Dzhumagulova, E. O. Shalenov, Y. A. Tashkenbayev, and T. S. Ramazanov, J. Plasma Phys. **88**, 905880119 (2022).
[37]K. N. Dzhumagulova, E. O. Shalenov, and G. L. Gabdullina, Phys. Plasmas **20**, 042702 (2013).
[38]E. O. Shalenov, K. N. Dzhumagulova, and T. S. Ramazanov, Phys. Plasmas **24**, 012101 (2017).
[39]K. N. Dzhumagulova, E. O. Shalenov, Y. A. Tashkenbayev, and T. S. Ramazanov, Phys. Plasmas **29**, 012101 (2022).
[40]E. O. Shalenov, S. Rosmej, H. Reinholz, G. Röpke, K. N. Dzhumagulova, and T. S. Ramazanov, Contrib. Plasma Phys. **57**, 486 (2017).
[41]S. K. Kodanova, T. S. Ramazanov, M. K. Issanova, G. N. Nigmetova, and Z. A. Moldabekov, Contrib. Plasma Phys. **55**, 271 (2015).
[42]S. K. Kodanova, M. K. Issanova, S. M. Amirov, T. S. Ramazanov, A. Tikhonov, and Z. A. Moldabekov, Matter Radiat. Extrem. **3**, 40 (2018).
[43]E. O. Shalenov, K. N. Dzhumagulova, T. S. Ramazanov, G. Röpke, and H. Reinholz, Phys. Plasmas **25**, 082706 (2018).
[44]E. O. Shalenov, K. N. Dzhumagulova, T. S. Ramazanov, H. Reinholz, and G. Röpke, Contrib. Plasma Phys. **59**, e201900024 (2019).
[45]M. K. Issanova, S. K. Kodanova, T. S. Ramazanov, N. K. Bastykova, Z. A. Moldabekov, and C.-V. Meister, Laser Part. Beams **34**, 457 (2016).
[46]S. K. Kodanova, T. S. Ramazanov, A. K. Khikmetov, and M. K. Issanova, Contrib. Plasma Phys. **58**, 946 (2018).
[47]M. M. Seisembayeva, H. Reinholz, E. O. Shalenov, M. N. Jumagulov, and K. N. Dzhumagulova, Contrib. Plasma Phys. **62**, e202200014 (2022).
[48]E. O. Shalenov, A. T. Nuraly, and K. N. Dzhumagulova, Contrib. Plasma Phys. **62**, e202200017 (2022).
[49]R. M. More, Adv. At. Mol. Phys. **21**, 305 (1985).
[50]A. Anders, S. Anders, A. Forster, and I. G. Brown, Plasma Sources Sci. Technol. **1**, 263 (1992).
[51]N. F. Mott, Rev. Mod. Phys. **40**, 677 (1968).
[52]J. P. Neirotti, P. Serra, and S. Kais, Phys. Rev. Lett. **79**, 3142 (1997).
[53]S. Kais and P. Serra, "Finite-size scaling for atomic and molecular systems," in *Advances in Chemical Physics*, edited by I. Prigogine and S. A. Rice (Wiley, New York, 2003), Vol. 125 Chap. 1, p. 1.
[54]C. S. Estienne, M. Busuttil, A. Moini, and G. W. F. Drake, Phys. Rev. Lett. **112**, 173001 (2014).
[55]H. E. Montgomery, Jr., K. D. Sen, and J. Katriel, Phys. Rev. A **97**, 022503 (2018).
[56]L. G. Jiao, R. Y. Zheng, A. Liu, H. E. Montgomery, Jr., and Y. K. Ho, Phys. Rev. A **105**, 052806 (2022).
[57]R. Bredow, T. Bornath, W.-D. Kraeft, and R. Redmer, Contrib. Plasma Phys. **53**, 276 (2013).
[58]W. Ebeling, Contrib. Plasma Phys. **56**, 163 (2016).
[59]M. M. Gombert and C. Deutsch, Phys. Lett. A **47**, 473 (1974).
[60]C. Deutsch, M. M. Gombert, and H. Minoo, Phys. Lett. A **66**, 381 (1978).
[61]C. Deutsch, M. M. Gombert, and H. Minoo, Phys. Lett. A **72**, 481 (1979).
[62]H. Minoo, M. M. Gombert, and C. Deutsch, Phys. Rev. A **23**, 924 (1981).
[63]L. G. Stanton and M. S. Murillo, Phys. Rev. E **91**, 033104 (2015).
[64]G. Yao and S.-I. Chu, Chem. Phys. Lett. **204**, 381 (1993).
[65]S.-I. Chu and D. A. Telnov, Phys. Rep. **390**, 1 (2004).
[66]L. Zhu, Y. Y. He, L. G. Jiao, Y. C. Wang, and Y. K. Ho, Int. J. Quantum Chem. **120**, e26245 (2020).
[67]A. Deloff, Ann. Phys. **322**, 1373 (2007).
[68]L. G. Jiao, H. H. Xie, A. Liu, H. E. Montgomery, Jr., and Y. K. Ho, J. Phys. B **54**, 175002 (2021).
[69]L. G. Jiao, L. Xu, R. Y. Zheng, A. Liu, Y. Z. Zhang, H. E. Montgomery, Jr., and Y. K. Ho, J. Phys. B **55**, 195001 (2022).
[70]L. Xu, L. G. Jiao, A. Liu, Y. C. Wang, H. E. Montgomery, Jr., Y. K. Ho, and S. Fritzsche, J. Phys. B **56**, 175002 (2023).
[71]X. H. Ji, Y. Y. He, L. G. Jiao, A. Liu, and Y. K. Ho, Phys. Lett. B **823**, 136718 (2021).
[72]"It should be noted that in calculating the ground state energy of the H-like Al ion, some plasma parameters near the critical bound region are in the potential forbidden region, where Eq. (6) fails. In these situations, the Eq. (15) of Ref. 32 is employed with the same asumption of $\lambda_{ei} = 0$."

[73]M. Klaus and B. Simon, Ann. Phys. **130**, 251 (1980).
[74]W. H. Press, S. A. Teukolsky, W. T. Vetterling, and B. P. Flannery, *Numerical Recipes in Fortran 77* (Cambridge University Press, New York, 1992).
[75]Y. Y. Qi, J. G. Wang, and R. K. Janev, Phys. Rev. A **80**, 032502 (2009).
[76]N. Mukherjee, C. N. Patra, and A. K. Roy, Phys. Rev. A **104**, 012803 (2021).
[77]Y. Y. He, Z. L. Zhou, L. G. Jiao, A. Liu, H. E. Montgomery, Jr., and Y. K. Ho, Phys. Rev. E **107**, 045201 (2023).
[78]J. Mitroy, M. S. Safronova, and C. W. Clark, J. Phys. B **43**, 202001 (2010).
[79]H. A. Bethe and E. E. Salpeter, *Quantum Mechanics of One- and Two-Electron Atoms* (Dover Publications, New York, 2008).
[80]S. Kar and Y. K. Ho, Phys. Rev. A **80**, 062511 (2009).
[81]Y.-C. Lin, C.-Y. Lin, and Y. K. Ho, Phys. Rev. A **85**, 042516 (2012).
[82]L. G. Jiao and Y. K. Ho, Phys. Rev. A **90**, 012521 (2014).
[83]S. Kar, Y.-S. Wang, and Y. K. Ho, Phys. Rev. A **99**, 042514 (2019).
[84]S. Bhattacharyya, J. K. Saha, and T. K. Mukherjee, Phys. Rev. A **91**, 042515 (2015).
[85]S. K. Chaudhuri, L. Modesto-Costa, and P. K. Mukherjee, Phys. Plasmas **23**, 053305 (2016).
[86]J. K. Saha, S. Bhattacharyya, and T. K. Mukherjee, Phys. Plasmas **23**, 092704 (2016).
[87]M. K. Bahar and A. Soylu, Phys. Plasmas **25**, 022106 (2018).
[88]S. Mondal, A. Sadhukhan, K. Sen, and J. K. Saha, J. Phys. B **56**, 155001 (2023).
[89]N. Das, A. Ghoshal, and Y. K. Ho, Phys. Plasmas **30**, 063511 (2023).
[90]N. Das, A. Ghoshal, and Y. K. Ho, "Helium atom embedded in non-ideal classical plasmas: Doubly excited singlet S states," Contrib. Plasma Phys. (published online 2024).
[91]S. Chakraborty and Y. K. Ho, Phys. Rev. A **77**, 014502 (2008).
[92]Y. Ning, Z.-C. Yan, and Y. K. Ho, Phys. Plasmas **22**, 013302 (2016).
[93]Y. Ning, Z.-C. Yan, and Y. K. Ho, Atoms **4**, 3 (2016).
[94]Z. Jiang, Y.-Z. Zhang, and S. Kar, Phys. Plasmas **22**, 052105 (2015).
[95]N. Masanta, A. Ghoshal, and Y. K. Ho, Phys. Plasmas **29**, 053505 (2022).
[96]M. Das, Phys. Plasmas **21**, 012709 (2014).
[97]S. Dutta, J. K. Saha, R. Chandra, and T. K. Mukherjee, Phys. Plasmas **23**, 042107 (2016).
[98]B. K. Sahoo and M. Das, Eur. Phys. J. D **70**, 270 (2016).
[99]M. Das and A. C. Pradhan, Phys. Plasmas **24**, 112706 (2017).
[100]S. K. Chaudhuri, P. K. Mukherjee, R. K. Chaudhuri, and S. Chattopadhyay, Phys. Plasmas **25**, 042705 (2018).
[101]M. Das, Eur. Phys. J. D **77**, 7 (2023).
[102]L. Sharma, B. K. Sahoo, P. Malkar, and R. Srivastava, Eur. Phys. J. D **72**, 10 (2018).
[103]L. G. Jiao, L. R. Zan, L. Zhu, J. Ma, and Y. K. Ho, Comput. Phys. Commun. **244**, 217 (2019).
[104]M.-A. Martínez-Sánchez, C. Martínez-Flores, R. Vargas, J. Garza, R. Cabrera-Trujillo, and K. D. Sen, Phys. Rev. E **103**, 043202 (2021).
[105]S. Lumb, S. Lumb, and V. Prasad, Phys. Rev. A **90**, 032505 (2014).
[106]S. Lumb, S. Lumb, and V. Prasad, Indian J. Phys. **89**, 13 (2015).
[107]S. L. Talwar, S. Lumb, K. D. Sen, and V. Prasad, J. Phys. B **56**, 225002 (2023).
[108]R. Joshi, Spectrosc. Lett. **55**, 192 (2022).
[109]R. Joshi, Eur. Phys. J. D **77**, 186 (2023).
[110]L. Bertini, M. Mella, D. Bressanini, and G. Morosi, Phys. Rev. A **69**, 042504 (2004).
[111]S. Kar and Y. K. Ho, Phys. Rev. A **86**, 014502 (2012).
[112]M. Pawlak, M. Bylicki, and P. K. Mukherjee, J. Phys. B **47**, 095701 (2014).
[113]A. F. Ordóñez-Lasso, F. Martín, and J. L. Sanz-Vicario, Phys. Rev. A **95**, 012504 (2017).
[114]A. Ghoshal and Y. K. Ho, J. Phys. B **42**, 175006 (2009).
[115]L. U. Ancarani and K. V. Rodriguez, Phys. Rev. A **89**, 012507 (2014).
[116]A. Sadhukhan, S. K. Nayek, and J. K. Saha, Eur. Phys. J. D **74**, 210 (2020).
[117]X. N. Li, Y. Z. Zhang, L. G. Jiao, Y. C. Wang, H. E. Montgomery, Jr., Y. K. Ho, and S. Fritzsche, Eur. Phys. J. D **77**, 96 (2023).